A Journal of the Gesellschaft Deutscher Chemiker

Angewandte International Edition GDCh Chemie

www.angewandte.org

Accepted Article

Title: A Supramolecular-Based Dual-Wavelength Phototherapeutic Agent with Broad Spectrum Antimicrobial Activity against Drug Resistant Bacteria

Authors: Zhi-Hao Yu, Xingshu Li, Fugui Xu, Xi-Le Hu, Jiatao Yan, Nahyun Kwon, Guo-Rong Chen, Tingting Tang, Xiaojing Dong, Yiyong Mai, Daijie Chen, Juyoung Yoon, Xiao-Peng He, and He Tian

To be cited as: *Angew. Chem. Int. Ed.* 10.1002/anie.201913506
Angew. Chem. 10.1002/ange.201913506

Link to VoR: http://dx.doi.org/10.1002/anie.201913506
http://dx.doi.org/10.1002/ange.201913506

WILEY-VCH

10.1002/anie.201913506

WILEY-VCH

A Supramolecular-Based Dual-Wavelength Phototherapeutic Agent with Broad Spectrum Antimicrobial Activity against Drug Resistant Bacteria

Zhi-Hao Yu,[†] Xingshu Li,[†] Fugui Xu,[†] Xi-Le Hu, Jiatao Yan, Nahyun Kwon, Guo-Rong Chen, Tingting Tang, Xiaojing Dong, Yiyong Mai,* Daijie Chen,* Juyoung Yoon,* Xiao-Peng He,* and He Tian

Abstract: *With the ever-increasing threat posed by the multi-drug resistance of bacteria, the development of non-antibiotic agents for the broad-spectrum eradication of clinically prevalent superbugs has remained a global challenge. Here, we demonstrate the simple supramolecular self-assembly of structurally defined graphene nanoribbons (GNRs) with a cationic porphyrin (Pp4N) to afford unique one-dimensional (1D) wire-like GNR superstructures coated with Pp4N nanoparticles. The developed Pp4N/GNR nanocomposite displayed excellent dual modal properties with significant reactive-oxygen-species (ROS) production (PDT) and temperature elevation (PTT) upon light irradiation at 660 and 808 nm, respectively. This combined approach proved synergistic, providing an impressive antimicrobial effect that led to complete annihilation of a wide spectrum of gram-positive, gram-negative, and drug resistant bacteria both in vitro and in vivo. This study also unveils the promise of GNRs as a new platform to develop dual-modal antimicrobial agents that are able to overcome antibiotic resistance*.

Introduction

The discovery of antibiotics in the early 1900s transformed human health with the ability to carry out surgical procedures with a minimalized risk in developing infection. The continued overuse coupled with the rapid spread of resistance mechanism has rendered many antibiotics, spanning multiple classes, inactive.[1] These so-called resistant superbugs have complicated disease treatment and some infections now fail to respond to conventional first-line treatments.[2,3] Pursuit of new treatments from the industrial sector has also declined in recent years due to their potential short shelf-lives, which has created a lack of eco-nomic incentives for pharmaceutical companies to develop new antibiotics-based treatments. Current estimates suggest that if no appropriate action is taken by 2050, approximately 10 million people could die directly or indirectly from a multidrug-resistant infection.[4-6] Alternative strategies able to circumvent antibiotic resistance are thus highly desirable.

In recent years, material-based approaches have found preliminary use for the treatment of bacterial infection.[7,8] Such methods have provided an approach able to produce the desired therapeutic effect with a reduced potential to develop drug resistant bacteria.[9-12] Recent efforts include the use of gold nanoparticles[13] and hybrids[14] that, upon light irradiation, produce reactive oxygen species (ROS) (photodynamic therapy – PDT) to eradicate bacteria. Another example combined gold nanorods and silver, a historically used antimicrobial agent,[15] for the image-guided treatment of bacterial infection.[16] Two-dimensional (2D) nanomaterials, such as graphene oxide (GO) and molybdenum disulfide (MoS_2), have also been reported as effective antimicrobial agents, due to their ability to catalyze the conversion of H_2O_2 into hydroxyl radical (OH•), a highly toxic ROS.[17-19] Related graphene-based nanocomposites, composed of graphene and Fe_2O_3 nanoparticles, have also shown a synergistic antibacterial effect upon light irradiation.[20] These elegant studies have provided inspiration for the development of effective material-based antimicrobial agents with these treatment strategies soon believed to become increasingly employed, when no effective traditional small-molecule antibiotics are available to be used.[21-23]

Current material-based systems with utility as effective antimicrobial therapies have been limited with those reported, failing to display general activity against multiple strains (i.e., gram-positive and gram-negative). We have recently reported structurally well-defined graphene nanoribbons (GNRs) grafted with poly(ethylene oxide) (PEO) chains to afford excellent dispersibility in aqueous solution (denoted as GNR-PEO2000, the number expresses the molar mass of PEO, see Figure 1).[24] These GNRs displayed high photothermal conversion efficiency, outperforming those of many conventional photothermal conversion nanomaterials, including GO, carbon nanotubes (CNTs), 2D MoS_2, and 2D MnO_2.[24] We thus envisaged that surface modification of a GNR-based nanocomposite with an effective photosensitizer (PS) would afford a dual modal light-based therapeutic strategy for broad spectrum treatment of

[*] Z. Yu, X. Hu, G. Chen, Prof. X. He, Prof. H. Tian
Key Laboratory for Advanced Materials and Joint International Research Laboratory of Precision Chemistry and Molecular Engineering, Feringa Nobel Prize Scientist Joint Research Center, School of Chemistry and Molecular Engineering, East China University of Science and Technology, 130 Meilong RD, Shanghai 200237, China
E-mail: xphe@ecust.edu.cn (X.-P. He)
Dr. F. Xu, Prof. Y. Mai
School of Chemistry and Chemical Engineering, Shanghai Key Laboratory of Electrical Insulation and Thermal Ageing, Shanghai Jiao Tong University,800 Dongchuan RD, Shanghai 200240, China
E-mail: mai@sjtu.edu.cn (Y. Mai)
X. Li, N. Kwon, Prof. J. Yoon
Department of Chemistry and Nanoscience, Ewha Womans University, Seoul 03760, Republic of Korea
E-mail: jyoon@ewha.ac.kr (J. Yoon)
Dr. J. Yan
Department of Polymer Materials, College of Materials Science and Engineering, Shanghai University, Shanghai 200444, China
Dr. T. Tang
Shanghai Key Laboratory of Orthopedic Implants, Department of Orthopedic Surgery, Shanghai Ninth People's Hospital, Shanghai Jiao Tong University School of Medicine, Shanghai 200011, China
Dr. X. Dong, Prof. D. Chen
Shanghai Institute of Pharmaceutical Industry, 285 Gebaini RD, Shanghai 201203, China
Prof. D. Chen
School of Pharmacy, Shanghai Jiao Tong University, 800 Dongchuan RD, Shanghai 200240, China
E-mail: cdj@sjtu.edu.cn (D. Chen)
[†] These authors contributed equally to this work.

Supporting information for this article is given via a link at the end of the document.

gram-positive and -negative bacteria, including multidrug-resistant bacteria.[25-28]

Here, we demonstrate the simple supramolecular self-assembly of a polycationic porphyrin (Pp4N) and GNR-PEO2000 to afford a new nanocomposite that combines both PDT and PTT functions for the treatment of bacterial infection. This convergent self-assembly approach yields "ready-to-go" dual-modal therapeutics without the need of further synthetic modification or purification.[29] As demonstrated by in vitro and in vivo studies, sequential irradiation with two different wavelengths enables the stepwise activation of PDT and PTT, maximizing therapeutic efficacy through a synergistic manner. To our knowledge, this is also the first exploration of GNRs in biological applications.

Results and Discussion

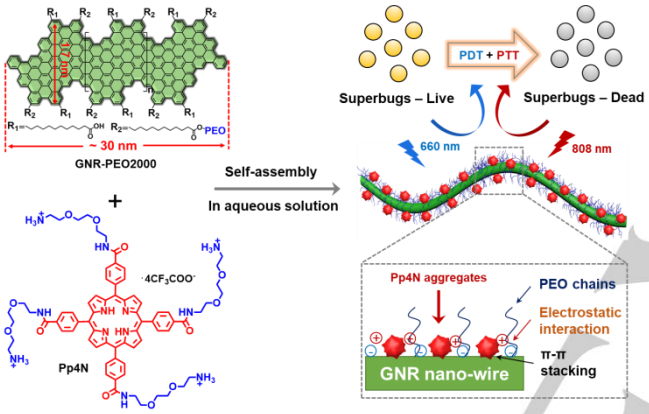

Figure 1. Structures of Pp4N (cationic porphyrin) and GNR-PEO2000 (water-dispersible GNRs with a PEO grafting percentage of 42%) used for self-assembly and double-light activated photodynamic and photothermal therapy of drug-resistant bacteria (superbugs).

Previous reports have shown strong electrostatic interactions are formed with cationic-based species and the negatively charged bacterial cell wall.[30,31] With this in mind, a porphyrin functionalized with four ammonium groups (termed as Pp4N) was synthesized, through modification of a previously reported method (Scheme S1).[32] Transmission electron microscopy (TEM) analysis of Pp4N in Tris-HCl buffer showed nanoparticle formation with an average diameter of 611 ± 59 nm (Fig. 2a). The fluorescence emission of Pp4N was significantly reduced due to the aggregation (Fig. S1a and S1b). GNR-PEO2000 was synthesized according to our previous protocol,[24,33-38] which was shown through TEM images to form 1D nanowires in aqueous solution (Fig. 2b). With both GNR-PEO2000 and Pp4N in hand, the electrostatic interaction between the positively charged Pp4N and the carboxyl groups on GNR-PEO2000 (with a grafting percentage of 42% for the PEO chains)[24] along with the potential π-π stacking would aid the formation of a novel self-assembled nanocomposite.[39]

Briefly, the self-assembled nanocomposite was prepared by the addition of the aqueous dispersion of GNR-PEO2000 to the solution of Pp4N, followed by sonication. As shown in Figure 2c and 2d, both TEM and atomic force microscopy (AFM) images revealed wire-like nanocomposites with Pp4N nanoparticles adsorbed on the surface. The composite nanowires possessed an average diameter of 50 ± 10 nm. This self-assembled structure was almost independent of the GNR-PEO and Pp4N concentrations as well as their ratios employed in the present study (Fig. S2). The slight difference in the superstructures formed under different ratios of Pp4N/GNR was the number density and the size of Pp4N particles attached on GNR nanowires. To show the superstructures more clearly, in Figure 2 we present the TEM and AFM images obtained from the sample with low Pp4N and GNR-PEO concentrations, on which the nanostructures may appear discretely. The TEM images for the samples with high concentrations (e.g. 40 μM) are given in Figure S2.

Raman spectra of both nanocomposite and GNR-PEO2000 displayed absorption peaks at 1600 cm^{-1} (G-band) and 1320 cm^{-1} (D-band), characteristic of the in-plane vibration of sp^2 carbon atoms (G-band) and the boundary defects of graphene (D-band), respectively (Fig. 2e). Their intensity ratio (I_D/I_G) is an important indicator for measuring the degrees of graphene disorder upon molecular interaction of graphene-based nanomaterials.[40,41] From this, we observed an increased I_D/I_G ratio for the composite (1.2) compared with that of GNR-PEO2000 (1.1), further indicating the formation Pp4N/GNR nanocomposite. Interestingly, the UV-Vis spectrum of the Pp4N/GNR (Fig. 2f), was shown to have superimposed characteristic peaks of both GNR-PEO2000 and Pp4N and the fluorescence intensity of Pp4N was shown to gradually increase with the addition of GNR-PEO2000 (Fig. 2g and Fig. S1c). This phenomenon further supports the adsorption of the Pp4N nanoparticles adsorbed onto the surface of GNR-PEO2000 through the reduction in their degree of aggregation, which diminishes the intrinsic ACQ effect. Overall, these spectroscopic results support the observed TEM images, in which monodispersed Pp4N particles with a significantly changed morphology and reduced sizes are detected on the surface of GNR nanowires, compared with that of individual Pp4N nanoparticles.[42]

To test the photodynamic properties of each component, the well-known ROS fluorescence probe, 9,10-diphenylanthracene, was used.[43] Irradiation of both Pp4N (Fig. S3b) and Pp4N/GNR (Fig. 3a and Fig. S3c) (660-nm laser) demonstrated significant ROS productivity, greater than that of Ce6, a clinically approved photosensitizer.[44] Through electronic paramagnetic resonance (EPR), the ROS produced was determined to be a mixture of singlet oxygen ($^1O_2$) and OH• [trapped by DMPO (5,5-dimethyl-1-pyrroline N-oxide)] (Fig. 3b).[21] These efforts further demonstrated the excellent ability of Pp4N/GNR to sensitize oxygen. Photostability experiments with Pp4N (Fig. S3e and S3h) and Pp4N/GNR (Fig. S3f and S3i) showed enhanced stability versus Ce6 (Fig. S3d and S3g) with Pp4N/GNR displaying the greatest photostability.

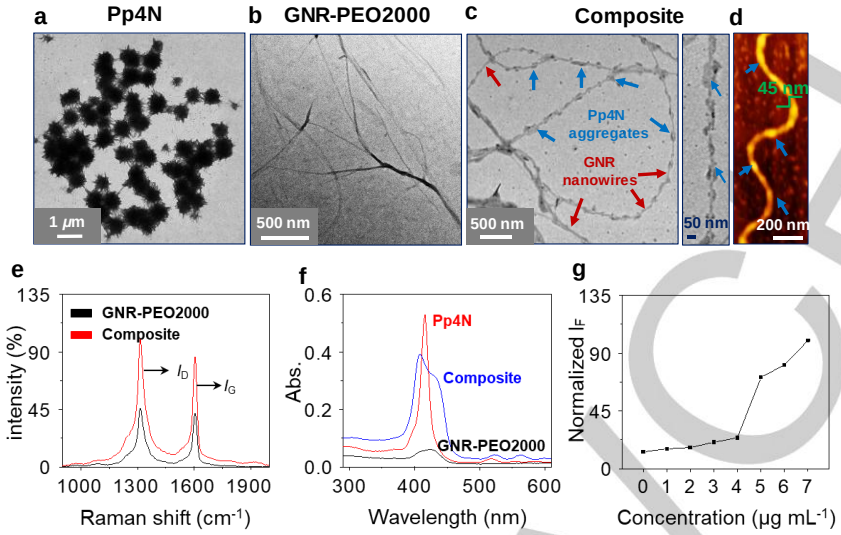

Figure 2. TEM images of (a) Pp4N (5 μM), (b) GNR-PEO2000 (2.5 μg mL^{-1}), and (c) the composite (Pp4N/GNR = 5 μM/2.5 μg mL^{-1}). (d) AFM height image of the composite (Pp4N/GNR = 5 μM/2.5 μg mL^{-1}). (e) Stacked Raman spectra and (f) typical UV-vis ab-sorption spectra of GNR-PEO2000 and the composite. The concentration of GNR-PEO2000 and Pp4N used was 7.5 μg mL^{-1} and 10 μM, respectively. (g) Plotting the fluorescence change of Pp4N (40 μM) in the presence of increasing GNR-PEO2000 concentration (1-7 μg mL^{-1}). λ_{ex} = 415 nm.

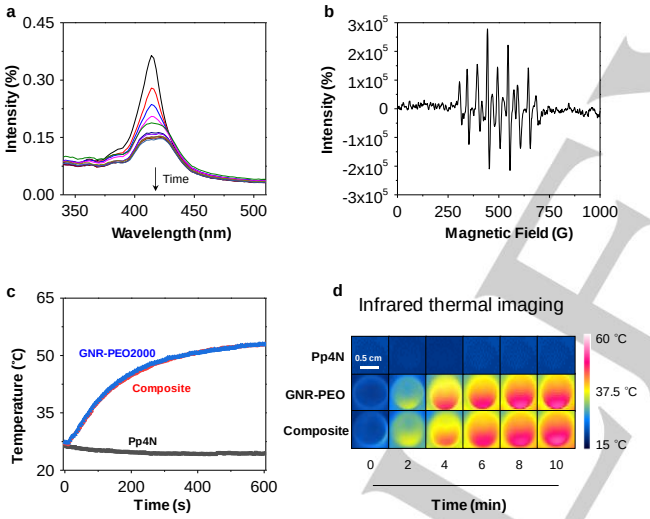

Figure 3. (a) Time-dependent UV-vis absorption intensity decreases of the composite (Pp4N/GNR-PEO2000 = 10 μM/7.5 μg mL^{-1}) measured by the structural change of DPA (10 μM) upon light irradiation (660 nm, 1 W cm^{-2}, 0-30 min; interval: 3 min). (b) EPR spectra of the composite (Pp4N/GNR-PEO2000 = 40 μM/30 μg mL^{-1}) measured by the structural change of DMPO (1 mM) upon light irradiation (660 nm, 1 W cm^{-2}, 15 min). (c) Temperature increase and (d) infrared thermal imaging of Pp4N (40 μM), GNR-PEO2000 (30 μg mL^{-1}) and the composite (Pp4N/GNR-PEO2000 = 40 μM/30 μg mL^{-1}) dissolved in a 96-well plate as monitored by an infrared thermal camera upon NIR light irradiation (808 nm, 1 W cm^{-2}, 10 min) with time.

Upon irradiation with an 808-nm laser,[24] both GNR-PEO2000 and Pp4N/GNR demonstrated a remarkable time-dependent temperature increase with the nanocomposite reaching 53 °C after only 10 min laser irradiation. In contrast, the temperature of the Pp4N solution remained unchanged (Fig. 3c and 3d). These outstanding photophysical and chemical properties of the Pp4N/GNR nanocomposites enabled its use as a dual-modal antimicrobial agent. Initially, the light-controlled antimicrobial capacity of Pp4N and GNR-PEO2000 were tested against Pseudomonas aeruginosa (P. aeruginosa). No significant dark toxicities were observed for both Pp4N (Fig. 4a, red columns) or GNR-PEO2000 (Fig. 4c, red columns). In contrast, the light irradiation of Pp4N (Fig. 4a, black columns, 660 nm) and GNR-PEO2000 (Fig. 4c, black columns, 880 nm), resulted in a concentration-dependent decrease in bacterial viability. From this, we determined that Pp4N (40 μM) or GNR-PEO2000 (20 μg mL^{-1}) alone led to the maximal bacteria suppression rate of 72.3% and 44.0%, respectively. In addition, the antibacterial activity of both Pp4N (Fig. 4b) and GNR-PEO2000 (Fig. 4d) were found to be dependent on the light irradiation time with the bacterial suppression level reaching an equilibrium at 15 min for both light sources (21.0% and 47.0% for 660-nm and 808-nm laser, respectively). A further increase in the irradiation time (30 min) did not improve the antibacterial activity of the composite, probably because the ROS productivity of Pp4N reached the maximum level upon exposure to 660 nm light for 15 min.

Subsequent analysis was focused on the antimicrobial performance of Pp4N/GNR, which combined PDT from Pp4N and PTT from GNR-PEO2000. As shown in Figure 4e and 4f, Pp4N/GNR demonstrated minimal dark toxicity, however, upon light irradiation, using the 808-nm laser first followed by the 660-nm laser, a significant reduction in bacterial viability (survival rate = 14.3%) was observed compared to the use of solely 660-nm (28.1%) or 880-nm laser (30.8%) (Fig. S4). This data is indicative of a synergistic combined PDT and PTT effect of the Pp4N/GNR nanocomposite. Interestingly, when the concentration of Pp4N was kept constant, the light-based

antimicrobial activity of Pp4N/GNR was shown dependent on the concentration of GNR-PEO2000 (Fig. 4e), with the use of 30 μg mL^{-1} GNR-PEO2000 leading to an almost complete suppression of bacteria (5.8%). In addition, the irradiation time of 15 min was shown to produce the maximum bacterial suppression rate for both light sources (Fig. 4f). The inherent non-toxicity of GNR-PEO2000 and Pp4N/GNR towards two normal cell lines was shown using a cell proliferation assay – 3T3-L1 (mouse embryonic fibroblast) and 293T (human embryonic kidney) (Fig. S5), thus demonstrating a potential applicability for clinical use.

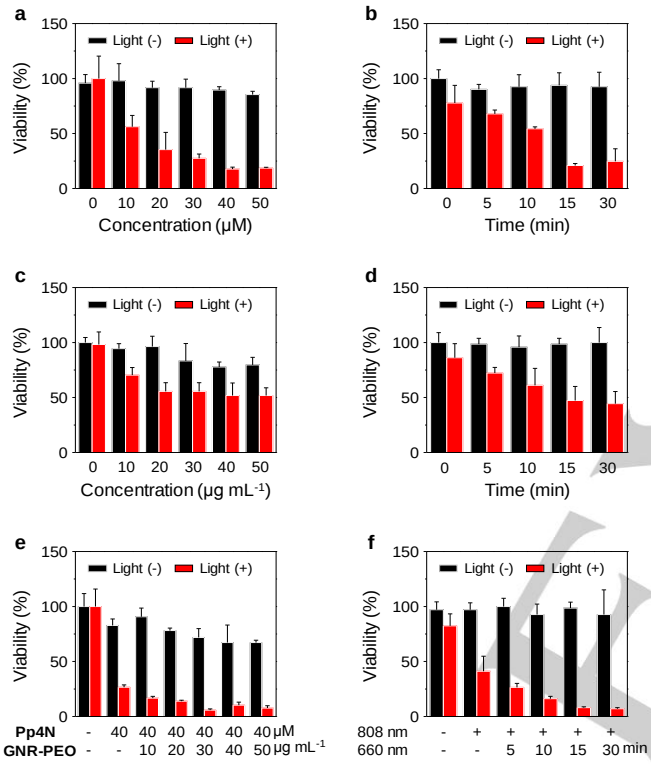

Figure 4. Relative bacterial viability of P. aeruginosa (ATCC 27853) in the absence or presence of Pp4N, GNR-PEO2000 and the composite with and without light irradiation P. aeruginosa incubated with (a) Pp4N (0-50 μM) treated with and without light irradiation (660 nm, 1 W cm^{-2}, 15 min). (b) Pp4N (40 μM) treated with and without light irradiation (660 nm, 1 W cm^{-2}, 0-30 min). (c) GNR-PEO2000 (0-50 μg mL^{-1}) treated with and without light irradiation (808 nm, 1 W cm^{-2}, 15 min). (d) GNR-PEO2000 (40 μg mL^{-1}) treated with and without light irradiation (808 nm, 1 W cm^{-2}, 0-30 min). (e) The composite (Pp4N/GNR = 40 μM/0-50 μg mL^{-1}) treated with and without light irradiation (808 nm, 1 W cm^{-2}, 15 min). (f) The composite (Pp4N/GNR = 40 μM/30 μg mL^{-1}) treated with and without light irradiation (808 nm, 1 W cm^{-2}, 0-30 min).

Pp4N/GNR was screened against a broad spectrum of gram-negative and gram-positive bacteria. The bacteria used include: Acinetobacter baumannii (A. baumannii, ATCC19606), Pseudomonas aeruginosa (P. aeruginosa, ATCC27853), Escherichia coli (E. coli, ATCC25922), Klebsiella pneumoniae (K. pneumonia, ATCC13883), methicillin-sensitive Staphylococcus aureus (MSSA, ATCC25923/CMCC26003/ATCC6538/ATCC29213), methicillin-resistant Staphylococcus aureus (MRSA, ATCC43300), Bacillus subtilis (B. subtilis, ATCC31002), Staphylococcus epidermidis (S. epidermidis, CMCC26069), γ-Streptococcus (CMCC32206) Staphylococcus lentus (S. lentus, CMCC26101), vancomycin resistant Enterococcus (VRE, ATCC51299), vancomycin sensitive Enterococcus (VSE, ATCC29212) (Fig. 5). Remarkably, the composite effectively suppressed the viability of all the selected superbugs. The inhibitory effect was also found greater for the gram-positive strains when compared to than that for the gram-negative strains. This is attributed to the strong electrostatic attraction between the positively charged Pp4N particles on the surface of the GNRs and the negatively charged cell walls of gram-positive bacteria.[45]

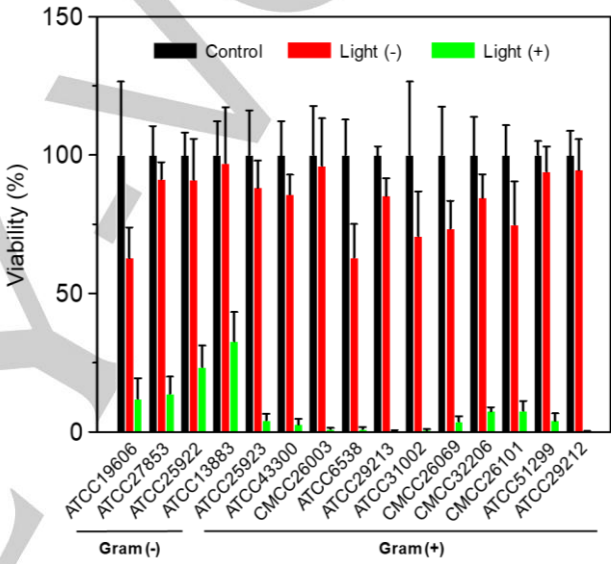

Figure 5. Relative bacterial viability of A. baumannii, P. aeruginosa, E. coli, K. pneumonia, MSSA, MRSA, B. subtilis, S. epidermidis, γ-Streptococcus, S. lentus, VRE, and VSE in the absence and presence of the composite (Pp4N/GNR = 40 μM/30 μg mL^{-1}) treated with and without 15 min of 808-nm light irradiation followed by 15 min of 660-nm light irradiation.

The antimicrobial ability of Pp4N/GNR was also tested using a dorsal-skin incised mouse model,[13] with the exposed area infected with A. baumannii (gram-negative) or MRSA (multidrug-resistant, gram-positive). The localization of each antimicrobial agent on the dorsal skin of mice was examined by photothermal imaging (Fig. 6). The control samples, without any agent and solely Pp4N, demonstrated a minimal temperature increase. GNR-PEO2000 and Pp4N/GNR exhibited a time-dependent temperature increase upon 808-nm laser irradiation (Fig. 6a, b for A. baumannii-infected mice and Fig. 6a, c for MRSA-infected mice, respectively) again demonstrating the PTT effect from GNR-PEO2000 and Pp4N/GNR. In contrast, the irradiation with 660 nm light could not trigger the composite to produce heat (Fig. S6a and S6b).

To prove the selective interaction of Pp4N/GNR with the pathogenic bacteria on the skin of the mice, a control imaging

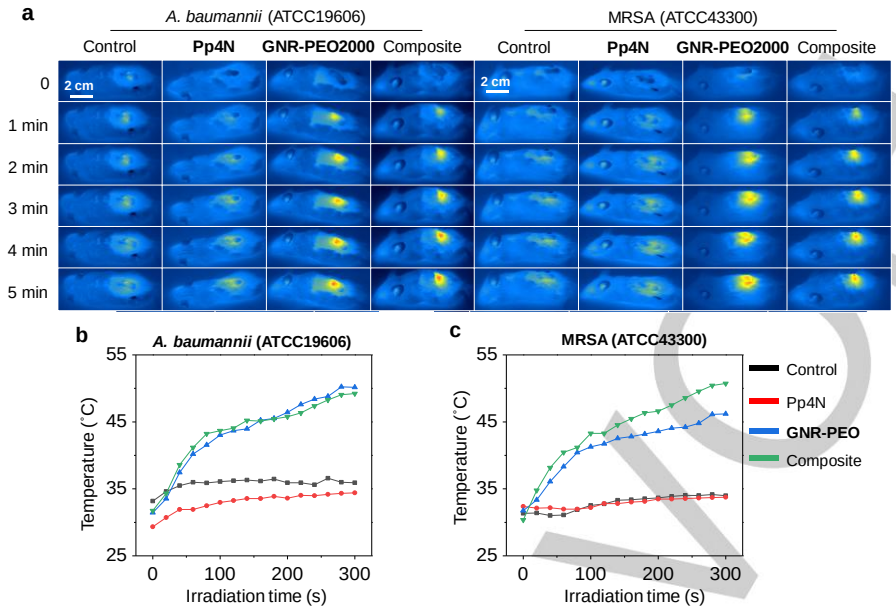

Figure 6. (a) Infrared thermal image of dorsal-skin incised mice with the wounded area infected by *A. baumannii* (ATCC 19606) and MRSA (ATCC 43300) in the absence or presence of Pp4N (40 μM), GNR-PEO2000 (30 μg mL^{-1}) and the composite (Pp4N/GNR = 40 μM/30 μg mL^{-1}) (the wounded area was treated with material followed by washing with phosphate buffered saline tree times) under NIR light irradiation for 5 min (808 nm;1 W cm^{-2}). Temperature increase on the wounds infected by (b) *A. baumannii* (ATCC 19606) and (c) MRSA (ATCC 43300) as monitored by the infrared thermal camera during NIR light irradiation with time.

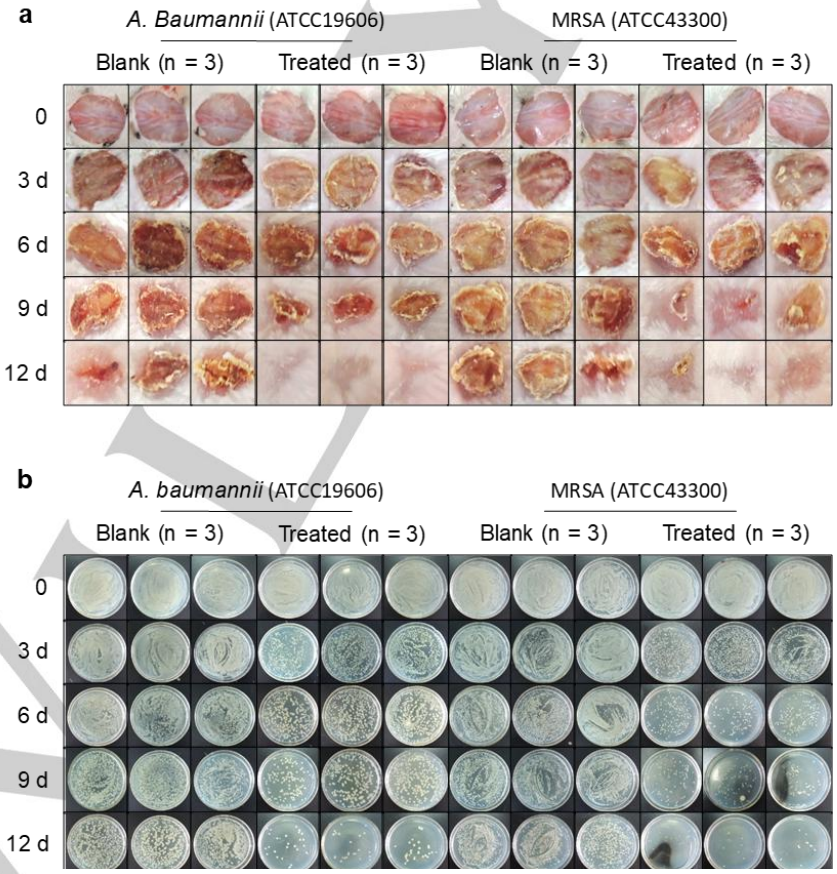

Figure 7. Light-driven antimicrobial effect of the composite (Pp4N/GNR = 40 μM/30 μg mL^{-1}) for *A. baumannii* (ATCC 19606) and MRSA (ATCC 43300)-infected wounds. (a) Representative photographs of the healing of *A. baumannii* and MRSA infected wounds with or without treatment of composite with time. (b) bacterial cultures obtained from the infected wounds without and with treatment of composite upon light irradiation (15 min of NIR light irradiation followed by 15 min of 660 nm light irradiation).

assay was carried out. Dorsal-skin incised mice with no bacterial infection were directly treated with Pp4N/GNR in which a similar time-dependent temperature increase was observed. However, subsequent washing of the uninfected dorsal skin led to a diminished temperature change being observed as a result of the removal of Pp4N/GNR (Fig. S6). This demonstrates the remarkable ability of Pp4N/GNR to associate with the bacteria on the mice over the mice skin.

Finally, experiments were performed using Pp4N/GNR to demonstrate its ability to treat the infected area on mice. The composite-treated infected area on the skins of mice were irradiated in the order of 660-nm to 808-nm laser, and then the wound healing process was monitored every 3 days. A. baumannii- and MRSA-infected wounds without treatment of the composite remained largely unhealed after a 12-day surveillance (Fig. 7a). However, wounds treated with Pp4N/GNR and irradiated, led to a gradual shrinkage in wound size during the 12-day period for both A. baumannii- and MRSA-infected mice. Further demonstrating the effectiveness of Pp4N/GNR, the plate counting method was used to quantify the amount of bacteria on the incised dorsal skin.[13] As shown in Fig. 7b, the bacterial colony did not decrease for the control group, however, both A. baumannii- and MRSA-infected groups displayed a sharp decrease in colony-forming units therefore demonstrating the effectiveness of Pp4N/GNR to be used as a photocontrolled antimicrobial material for the eradication of drug-resistant bacteria on live animals.

To prove the synergistic effect of the combination of Pp4N with GNR-PEO2000 for bacterial eradication, we employed the combination index (CI) to quantitatively depict synergism (CI < 1), additive effect (CI = 1), and antagonism (CI > 1).[46] We treated *A. baumannii* and MRSA that were used for *in vivo* study with Pp4N, GNR-PEO2000 and Pp4N/GNR at three different concentrations: Pp4N (40, 20 and 10 μM) irradiated with 660 nm light (1 W cm^{-2}) for 15 min, GNR-PEO2000 (30, 15 and 7.5 μg mL^{-1}) irradiated with 808 nm light (1 W cm^{-2}) for 15 min, and the composite (Pp4N/GNR = 40 μM/30 μg mL^{-1}, 20 μM/15 μg mL^{-1} and 10 μM/7.5 μg mL^{-1}) irradiated with NIR light (808 nm) for 15 min followed by 660 nm light for 15 min. Through the Fa-CI plot simulated by CompuSyn, we determined a CI value of 0.18 and 0.72 (CI < 1) for the antibacterial effect of Pp4N/GNR against *A. baumannii* and MRSA, respectively (Fig. S7 and Table S1). This result quantitatively supports the synergistic antibacterial effect of the Pp4N/GNR composite.

Conclusion

In summary, we have demonstrated the development of a supramolecular self-assembled nanocomposite displaying dual-modal PDT/PTT activity for the light-based treatment against a wide spectrum of drug resistant gram-positive and gram-negative bacteria strains. These Pp4N/GNR self-assembled superstructures also proved photostable with minimal toxicity to human cells and efficacious activity in bacterial infection mice models. The present results highlight how the synergistic combination of multiple therapeutic mechanisms can enhance material-based antimicrobials. New systems applying such an approach may thus find utility in addressing the growing need for non-antibiotic agents.

Acknowledgements

The authors thank Prof. Xinliang Feng at Technische Universität Dresden for help with some measurements. A. C. Sedgwick at UT Austin is appreciated for help in editing this manuscript. Financial support from the Natural Science Foundation of China (21788102, 91853201, 21774076, 51573091, 21722801 and 21776078), the National Research Foundation of Korea (NRF), which was funded by the Korea government (MSIP) (2012R1A3A2048814), the Shanghai Municipal Science and Technology Major Project (2018SHZDZX03), the Program of Shanghai Academic Research Leader (19XD1421700), and the Program of Shanghai Eastern Scholar are gratefully acknowledged. The Instrumental Analysis Center of Shanghai Jiao Tong University is also acknowledged for some measurements.

Conflict of interest

The authors declare no conflict of interest.

Keywords: antimicrobial • graphene nanoribbon • porphyrin • phototherapy • supermolecular structure

[1] P. Kardas, S. Devine, A. Golembesky, C. Roberts, *Int. J. Antimicrob. Agents* **2005**, *26*, 106-113.

[2] B. Y. Li, T. J. Webster, *J Orthop. Res*. **2018**, *36*, 22-32.

[3] D. Genne, L. Kaiser, T. N. Kinge, D. Lew, *Clin. Microbiol. infect*. **2003**, *9*, 949-954.

[4] S. B. Levy, B. Marshall, *Nat. Med.* **2004**, *10*, 122-129.

[5] E. D. Brown, G. D. Wright, *Nature* **2016**, *529*, 336-343.

[6] C. Willyard, *Nature* **2017**, *543*, 15-15.

[7] A. Gupta, S. Mumtaz, C.-H. Li, I. Hussain, V. M. Rotello, *Chem. Soc. Rev*. **2019**, *48*, 415-427.

[8] R. Kurapati, K. Kostarelos, M. Prato, A. Bianco, *Adv. Mater*. **2016**, *28*, 6052-6074.

[9] X. Li, S. Lee, J. Yoon, *Chem. Soc. Rev.* **2018**, *47*, 1174-1188.

[10] X. Li, H. Bai, Y. Yang, J. Yoon, S. Wang, X. Zhang, *Adv. Mater.* **2019**, *31*, 1805092-1805120.

[11] X. Li, D. Lee, J.-D. Huang, J. Yoon, *Angew. Chem. Int. Ed*. **2018**, *57*, 9885-9890. *Angew. Chem.* **2018**, *130*, 10033-10038.

[12] S. Y. Lee. H. Cheng, M. Y. Chi, Q. L. Xu, X. Q. Chen, C.-Y. Eom, T. D. James, *Biosens. Bioelectron*. **2016**, *77*, 1016-1019.

[13] W.-Y. Chen, H.-Y. Chang, J.-K. Lu, Y.-C. Huang, S. G. Harroun, Y.-T. Tseng, Y.-J. Li, C.-C. Huang, H.-T. Chang, *Adv. Funct. Mater.* **2015**, *25*, 7189-7199.

[14] W. He, H.-K. Kim, W. G. Wamer, D. Melka, J. H. Callahan, J.-J. Yin, *J. Am. Chem. Soc.* **2014**, *136*, 750-757.

[15] L. Rizzello, P. P. Pompa, *Chem. Soc. Rev*. **2014**, *43*, 1501-1518.

[16] T. Kim, Q. Zhang, J. Li, L. Zhang, J. V. Jokerst, *ACS Nano* **2018**, *12*, 5615-5625.

[17] H. Sun, N. Gao, K. Dong, J. Ren, X. Qu, *ACS Nano* **2014**, *8*, 6202-6210.

[18] C. D. Vecitis, K. R. Zodrow, S. Kang, *ACS Nano* **2010**, *4*, 5471-5479.

[19] W. Hu, C. Peng, W. Luo, M. Lv, X. Li, D. Li, Q. Huang, *ACS Nano* **2010**, *4*, 4317-4323.

[20] M.-C. Wu, A. R. Deokar, J.-H. Liao, P.-Y. Shih, Y.-C. Ling, *ACS Nano* **2013**, *7*, 1281-1290.

[21] C. Mao, Y. Xiang, X. Liu, Z. Cui, X. Yang, K. W. K. Yeung, H. Pan, X. Wang, P. K. Chu, S. Wu, *ACS Nano* **2017**, *11*, 9010-9021.

[22] X.-W. Huang, J.-J. Wei, T. Liu, X.-L. Zhang, S.-M. Bai, H.-H. Yang, *Nanoscale* **2017**, *9*, 17193-17198.

[23] Y. Wang, H. Wang, D. Liu, S. Song, X. Wang, H. Zhang, *Biomaterials* **2013**, *34*, 7715-7724.

[24] Y. Huang, W.-T. Dou, F. Xu, H.-B. Ru, Q. Gong, D. Wu, D. Yan, H. Tian, X.-P. He, Y. Mai, X. Feng, *Angew. Chem. Int. Ed.* **2018**, *57*, 3366-3371. *Angew. Chem.* **2018**, *130*, 3424-3429.

[25] K. Liu, Y. Liu, Y. Yao, H. Yuan, S. Wang, Z. Wang, X. Zhang, *Angew. Chem. Int. Ed.* **2013**, *52*, 8285-8289.

[26] J. P. Celli, B. Q. Spring, I. Rizvi, C. L. Evans, K. S. Samkoe, S. Verma, B. W. Pogue, T. Hasan, *Chem. Rev.* **2010**, *110*, 2795-2838.

[27] L. Tan, J. Li, X. Liu, Z. Cui, X. Yang, K. W. K. Yeung, H. Pan, Y. Zheng, X. Wang, S. Wu, *Small* **2018**, *14*, 1703197-1703208.

[28] A. P. Castano, P. Mroz, M. R. Hamblin, *Nat. Rev.* **2006**, *6*, 535-545.

[29] A. Galstyan, R. Schiller, U. Dobrindt, *Angew. Chem. Int. Ed*. **2017**, *56*, 10362-10366. *Angew. Chem.* **2017**, *129*, 10498-10502.

[30] D. Hu, H. Li, B. Wang, Z. Ye, W. Lei, F. Jia, Q. Jin, K.-F. Ren, J. Ji, *ACS Nano* **2017**, *11*, 9330-9339.

[31] C. Korupalli, C.-C. Huang, W.-C. Lin, W.-Y. Pan, W.-L. Wan, M.-J. Li, Y. Chang, H.-W. Sun, *Biomaterials* **2017**, *116*, 1-9.

[32] Gianferrara, T.; Bergamo, A.; Bratsos, I.; Milani, B.; Spagnul, C.; Sava, G.; Alessio, E. *J. Med. Chem*. **2010**, *53*, 4678–4690.

[33] Y. J. Huang, F. G. Xu, L. C. Ganzer, F. V. A. Camargo, T. Nagahara, J. Teyssandier, H. V. Gorp, K. Basse, L. A. Straasø, V. Nagyte, C. Casiraghi, M. R. Hansen, S. D. Feyter, D. Yan, K. Müllen, X. L. Feng, G. Cerullo, Y. Mai, *J. Am. Chem. Soc.* **2018**, *140*, 10416–10420.

[34] W. Niu, J. Liu, Y. Mai, K. Müllen, X. Feng, *Trends in Chemistry* **2019**, *1*, 549-558.

[35] D. D. Wu, F. G. Xu, Y. J. Huang, C. S. Chen, C. Y. Yu, X. L. Feng, D. Y. Yan, Y. Mai, *Macromolecules* **2018**, *51*, 161–172.

[36] Y. J. Huang, Y. Mai, U. Beser, J. Teyssandier, G. Velpula, H. V. Gorp, L. A. Straasø, M. R. Hansen, D. Rizzo, C. Casiraghi, R. Yang, G. Y. Zhang, D. Q. Wu, F. Zhang, D. Y. Yan, S. D. Feyter, K. Müllen, X. L Feng,. *J. Am. Chem. Soc.* **2016**, *138*, 10136-10139.

[37] Huang, Y. J.; Mai, Y.; Yang, X. W.; Beser, U.; Liu, J. Z.; Zhang, F.; Yan, D. Y.; Müllen, K.; Feng, X. L. *J. Am. Chem. Soc*. **2015**, *137*, 11602-11605.

[38] F. G. Xu, C. Yu, A. Tries, H. Zhang, M. Kläui, K. Basse, M. R. Hansen, N. Bilbao, M. Bonn, H. I. Wang, Y. Mai, *J. Am. Chem. Soc.* **2019**, *141*, 10972-10977.

[39] Li. Wu, J. Wang, L. Feng, J. Ren, W. Wei, X. Qu, *Adv. Mater.* **2012**, *24*, 2447-2452.

[40] H.-L. Zhang, X.-L. Wei, Y. Zang, J.-Y. Cao, S. Liu, X.-P. He, Q. Chen, Y.-T. Long, J. Li, G.-R. Chen, K. Chen, *Adv. Mater.* **2013**, *25*, 4097-4101.

[41] A. Jorio, E. H. M. Ferreira, M. V. O. Moutinho, F. Stavale, C. A. Achete, R. B. Capaz, *Phys. Status Solidi B* 2**010**, *247*, 2980-2982.

[42] X. Yan, G. Niu, J. Lin, A. J. Jin, H. Hu, Y. Tang, Y. Zhang, A. Wu, J. Lu, S. Zhang, P. Huang, B. Shen, X. Chen, *Biomaterials* **2015**, *42*, 94-102.

[43] Z. J. Diwu, J. W. Lown, *J. Photochem. Photobiol. A: Chem*. **1992**, *64*, 273-287.

[44] Z. Y. Sun, L.-P. Zhang, F. P. Wu, Y. X Zhao, *Adv. Funct. Mater*. **2017**, *27*, 1704079-1704100.

[45] C. Zhu, Q. Yang, L. Liu, F. Lv, S. Li, G. Yang, S. Wang, *Adv. Mater.* **2011**, *23*, 4805-4810.

[46] T.-C. Chou, *Cancer Res.* **2010**, *15*, 440-446.

10.1002/anie.201913506

WILEY-VCH

RESEARCH ARTICLE

This paper reports the simple supramolecular self-assembly of a polycationic porphyrin and water-dispersible graphene nanoribbons to afford a new nanocomposite that combines both PDT and PTT functions for the treatment of bacterial infection. The supramolecular nanocomposite exhibits an impressive antimicrobial effect that leads to complete annihilation of a wide spectrum of gram-positive, gram-negative, and drug resistant bacteria both in vitro and in vivo. The study also unveils the promise of graphene nanoribbons as a new platform for the development of dual-modal antimicrobial agents that are able to overcome antibiotic resistance.

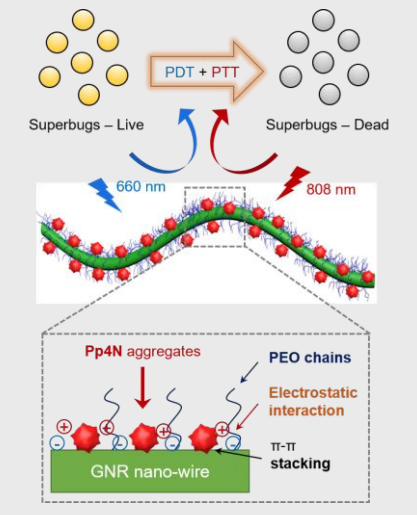

Zhi-Hao Yu,† Xingshu Li,† Fugui Xu,† Xi-Le Hu, Jiatao Yan, Nahyun Kwon, Guo-Rong Chen, Tingting Tang, Xiaojing Dong, Yiyong Mai, Daijie Chen,* Juyoung Yoon,* Xiao-Peng He,* and He Tian*

Page No. – Page No.
A Supramolecular-Based Dual-Wavelength Phototherapeutic Agent with Broad Spectrum Antimicrobial Activity against Drug Resistant Bacteria